


Single-shot measurement of overall degree of spectral coherence: Bulk-generated supercontinuum case

Debanjan Show,¹ Atri Halder,¹ Tommi K. Hakala,^{1,*} and Matias Koivurova^{2,3,†}

¹*Department of Physics and Mathematics, University of Eastern Finland, P.O. Box 111, FI-80101 Joensuu, Finland*

²*Tampere Institute for Advanced Study, Tampere University, 33100 Tampere, Finland*

³*Faculty of Engineering and Natural Sciences, Tampere University, 33720 Tampere, Finland*

 (Received 23 December 2021; revised 9 March 2022; accepted 9 March 2022; published 29 March 2022)

Spectral and temporal correlations determine the majority of pulse properties, and a high degree of coherence is needed for minimizing the pulse length. However, there is no simple way to quantify these correlations experimentally, and nonlinear methods are often required. In this paper, we confirm an earlier proposed experiment [Koivurova *et al.*, *Opt. Lett.* **44**, 522 (2019)] that can accurately estimate the spectral degree of coherence of arbitrary nonstationary fields. The method is entirely linear and can retrieve the quasicohherent contribution of the spectral correlation function. In particular, the method can be used to measure the overall degree of spectral coherence in a single-shot manner. We first establish the theoretical framework behind the method and experimentally test it for a bulk-generated supercontinuum. Our experimental results are in good agreement with the theory and confirm our earlier numerical findings [Halder *et al.*, *Photon. Res.* **7**, 1345 (2019)]. Moreover, the results yield insight into supercontinuum generation in bulk material.

DOI: [10.1103/PhysRevB.105.104310](https://doi.org/10.1103/PhysRevB.105.104310)

I. INTRODUCTION

A complete characterization of temporal and spectral coherence properties of nonstationary light fields, such as supercontinuum pulses, requires knowledge of the two-time mutual coherence function (MCF) and the two-frequency cross-spectral density function (CSD), respectively [1–8]. To date, there is no measurement technique by which one could measure the MCF and CSD directly. In practice, one can measure individual pulses, utilizing nonlinear pulse measurement techniques such as frequency-resolved optical gating (FROG) [9] or spectral phase interferometry for direct electric-field reconstruction (SPIDER) [10,11], and then construct the two-point correlation functions numerically [12]. This is a time-consuming process, although it yields a large amount of correlation information. However, one is often concerned with only the overall degree of spectral coherence of the field, because a completely coherent field produces the shortest possible pulse [11,13–15] and the most stable optical frequency combs [16–20]. The overall degree of coherence can be found as a root-mean-square average of the absolute value of either the CSD or MCF. In other words, the extremely time-consuming process of finding the data for a large correlation function is used to generate a single number that evaluates the overall coherence of the field.

In Ref. [21] a cross-correlation-type experiment was proposed to find quantitative information about the coherence properties of such pulsed fields. The method was applied to numerically generated supercontinuum realizations, and it

was proposed that it is possible to reconstruct the quasicohherent part of the CSD in this manner. Additionally, in Ref. [22] the coherence properties of bulk-generated supercontinuum pulses were investigated numerically, where it was shown that their dynamics are more involved than in the case of a fiber-generated supercontinuum. In particular, it was shown that the temporal and spectral coherence properties of bulk-generated supercontinuum pulses were high even if the pumping was much higher than the threshold of supercontinuum generation, in contrast to the fiber case.

Most of current supercontinuum research has focused on fiber-generated supercontinua, due to the simplification of the physical picture when the spatial degree of freedom is removed. The spatial confinement also leads to lower threshold energies, and supercontinuum generation has been observed even with high-power continuous wave pumps [23]. However, the dynamics of a fiber supercontinuum lead to a chaotic time evolution when the pump power is increased above a certain threshold, leading to low temporal coherence [2,3,12]. Moreover, fibers may be susceptible to optical damage, and therefore it is difficult to reach large supercontinuum energies. On the other hand, the dynamics in the bulk case are entirely different, and the power can be scaled by increasing the spatial width of the pump pulse. Therefore there can be instances where bulk media are preferred over fiber.

In the present study, we have experimentally verified some of the results presented in Ref. [22], by employing the technique suggested in Ref. [21]. Moreover, we have gained insight into the dynamics of the bulk-generated supercontinuum. We first theoretically show that the cross correlation can in fact retrieve the overall degree of spectral coherence in a single measurement, requiring only minimal numerical processing. We then move on to experimentally test the

*tommi.hakala@uef.fi

†matias.koivurova@tuni.fi

method with bulk-generated supercontinuum pulses that feature a spectral width of up to ~ 300 nm. The overall degree of spectral coherence was extracted with a single measurement, and it was even possible to approximately reconstruct the quasicohherent contribution to the CSD from measured temporal data. Our results show evidence that in the case of a bulk-generated supercontinuum, the different nonlinear processes have entirely different coherence properties when compared with the fiber case.

II. THEORY OF MEASUREMENT

Considering pulses propagating towards the positive half-space $z > 0$, we denote a collimated scalar field at the transverse position $\boldsymbol{\rho} = (x, y)$ by the complex analytic signal $E(\boldsymbol{\rho}; t)$, where t is the time in the moving reference frame of the pulse, such that $t = 0$ is at the center of the pulse. The spectral domain field, $E(\boldsymbol{\rho}; \omega)$, is attained via Fourier transform,

$$E(\boldsymbol{\rho}; t) = \mathcal{F}\{E(\boldsymbol{\rho}; \omega)\} = \frac{1}{2\pi} \int_0^\infty E(\boldsymbol{\rho}; \omega) \exp(-i\omega t) d\omega, \quad (1)$$

where the lower limit is zero due to analyticity. Let us take two different time domain pulses from the same pulse train, $E_i(\boldsymbol{\rho}; t)$ and $E_j(\boldsymbol{\rho}; t)$, where $i \neq j$, and correlate them. Such a situation may be experimentally encountered, for example, when the repetition rate of a pulsed laser is high enough for one to employ an unbalanced Michelson interferometer, such as in Ref. [12].

In this case, the temporal field exiting the interferometer is given by

$$E(\boldsymbol{\rho}; t, \Delta t) = E_i(\boldsymbol{\rho}; t) + E_j(\boldsymbol{\rho}; t + \Delta t), \quad (2)$$

where the time delay, Δt , can be chosen such that the overlap between the pulses varies. If we place a detector at the exit port of the interferometer, it will measure the time-integrated intensity pattern, i.e., $I(\boldsymbol{\rho}; \Delta t) = \int \langle |E(\boldsymbol{\rho}; t, \Delta t)|^2 \rangle dt$, which takes on the form

$$I(\boldsymbol{\rho}; \Delta t) = I_i(\boldsymbol{\rho}) + I_j(\boldsymbol{\rho}) + 2 \operatorname{Re} \left\{ \int \langle E_i^*(\boldsymbol{\rho}; t) E_j(\boldsymbol{\rho}; t + \Delta t) \rangle dt \right\}, \quad (3)$$

where I_i and I_j stand for the individual time-integrated pulse intensities, Re is the real part, and angle brackets denote ensemble averaging over a large number of pulses. The last part of this relation is the cross-correlation term, $\langle X(\boldsymbol{\rho}; \Delta t) \rangle = \int \langle E_i^*(\boldsymbol{\rho}; t) E_j(\boldsymbol{\rho}; t + \Delta t) \rangle dt$, and therefore we can write

$$I(\boldsymbol{\rho}; \Delta t) = I_i(\boldsymbol{\rho}) + I_j(\boldsymbol{\rho}) + 2|\langle X(\boldsymbol{\rho}; \Delta t) \rangle| \cos[\Phi(\boldsymbol{\rho}; \Delta t)], \quad (4)$$

where $\Phi(\boldsymbol{\rho}; \Delta t)$ is the phase of the cross correlation, which can be found from the positions of the interference fringes. The absolute value of the cross-correlation term is encoded into the visibility of interference fringes.

In Ref. [21], it was shown that the cross correlation is related to the quasicohherent part of the power spectrum, as in

$$\langle X(\boldsymbol{\rho}; \Delta t) \rangle \approx \mathcal{F}\{S_{\text{qc}}(\boldsymbol{\rho}; \omega)\}, \quad (5)$$

with $S_{\text{qc}}(\boldsymbol{\rho}; \omega) = |\langle E(\boldsymbol{\rho}; \omega) \rangle|^2$ being the quasicohherent part of the spectrum [2,3,12], evaluated at the spatial position $\boldsymbol{\rho}$. The approximation becomes better the more pulse pairs the measurement includes. Hence we can extract the quasicohherent part of the spectrum with

$$S_{\text{qc}}(\boldsymbol{\rho}; \omega) = \mathcal{F}^{-1}\{|\langle X(\boldsymbol{\rho}; \Delta t) \rangle| \cos[\Phi(\boldsymbol{\rho}; \Delta t)]\} \\ = \mathcal{F}^{-1}\{[I(\boldsymbol{\rho}; \Delta t) - I_i(\boldsymbol{\rho}) - I_j(\boldsymbol{\rho})]/2\}, \quad (6)$$

and \mathcal{F}^{-1} denotes the inverse Fourier transform. Since the inverse Fourier transform is over a real function, the result will contain duplicate information at negative and positive frequencies.

The CSD—which contains all spectral correlation properties of the field—can be divided into two contributions; that is,

$$W(\boldsymbol{\rho}, \boldsymbol{\rho}; \omega_1, \omega_2) = W_{\text{qc}}(\boldsymbol{\rho}, \boldsymbol{\rho}; \omega_1, \omega_2) + W_{\text{qs}}(\boldsymbol{\rho}, \boldsymbol{\rho}; \omega_1, \omega_2), \quad (7)$$

where the subscripts “qc” and “qs” stand for quasicohherent and quasistationary, respectively. The special characteristic of these two contributions is that they are separable in different coordinate systems; the quasicohherent part separates in the absolute coordinates (ω_1, ω_2) , whereas the quasistationary part can be separated in average and difference coordinates $(\bar{\omega}, \Delta\omega)$, where $\bar{\omega} = (\omega_1 + \omega_2)/2$ and $\Delta\omega = \omega_2 - \omega_1$. Naturally, the higher the degree of coherence is, the more weight the quasicohherent part has, and we will thus be focusing on this contribution.

We can use the quasicohherent part of the power spectrum to estimate the coherent contribution of the CSD, as in

$$|W_{\text{qc}}(\boldsymbol{\rho}, \boldsymbol{\rho}; \omega_1, \omega_2)| \approx \sqrt{S_{\text{qc}}(\boldsymbol{\rho}; \omega_1)} \sqrt{S_{\text{qc}}(\boldsymbol{\rho}; \omega_2)}, \quad (8)$$

as well as the normalized spectral degree of coherence

$$|\mu_{\text{qc}}(\boldsymbol{\rho}, \boldsymbol{\rho}; \omega_1, \omega_2)| \approx \frac{\sqrt{S_{\text{qc}}(\boldsymbol{\rho}; \omega_1)} \sqrt{S_{\text{qc}}(\boldsymbol{\rho}; \omega_2)}}{\sqrt{S(\boldsymbol{\rho}; \omega_1)} \sqrt{S(\boldsymbol{\rho}; \omega_2)}}, \quad (9)$$

where the overall spectral density, $S(\boldsymbol{\rho}; \omega)$, can be found with some other method, such as autocorrelation or a spectrometer. Unfortunately, as these quantities do not carry any phase information, the MCF cannot be constructed from these data.

Usually, one wishes to quantify the overall degree of coherence with some single numerical value. In the case of bulk-generated supercontinuum light, this value may depend on the spatial position, since the pump power varies across the beam. Therefore we can define a position-dependent overall degree of spectral coherence as

$$\bar{\mu}(\boldsymbol{\rho})^2 = \frac{\iint |W(\boldsymbol{\rho}, \boldsymbol{\rho}; \omega_1, \omega_2)|^2 d\omega_1 d\omega_2}{\iint S(\boldsymbol{\rho}; \omega_1) S(\boldsymbol{\rho}; \omega_2) d\omega_1 d\omega_2}, \quad (10)$$

which is constrained between 0 and 1, signifying complete spectral incoherence and coherence, respectively. This can be simplified by substituting from Eq. (8) and noting that the integrals are separable, thus yielding

$$\bar{\mu}(\boldsymbol{\rho}) \approx \frac{\int_0^\infty S_{\text{qc}}(\boldsymbol{\rho}; \omega) d\omega}{\int_0^\infty S(\boldsymbol{\rho}; \omega) d\omega}. \quad (11)$$

In practical terms, Eq. (11) is simply the ratio between the coherent power and the overall power.

Furthermore, if we replace $S_{qc}(\boldsymbol{\rho}; \omega)$ with its inverse Fourier transform and note that $\int S(\boldsymbol{\rho}; \omega) d\omega = \sqrt{I_i(\boldsymbol{\rho})I_j(\boldsymbol{\rho})}$, we get the expression

$$\bar{\mu}(\boldsymbol{\rho}) \approx \frac{\int_0^\infty \int_{-\infty}^\infty \langle X(\boldsymbol{\rho}; \Delta t) \rangle \exp(i\omega \Delta t) d\Delta t d\omega}{\sqrt{I_i(\boldsymbol{\rho})I_j(\boldsymbol{\rho})}}. \quad (12)$$

We can now change the order of integration and compute the ω integral first, yielding

$$\bar{\mu}(\boldsymbol{\rho}) \approx \frac{\int_{-\infty}^\infty \langle X(\boldsymbol{\rho}; \Delta t) \rangle \delta(\Delta t) d\Delta t}{\sqrt{I_i(\boldsymbol{\rho})I_j(\boldsymbol{\rho})}}, \quad (13)$$

where $\delta(x)$ is the Dirac delta function. Performing the last integral gives the straightforward result

$$\bar{\mu}(\boldsymbol{\rho}) \approx \frac{\langle X(\boldsymbol{\rho}; 0) \rangle}{\sqrt{I_i(\boldsymbol{\rho})I_j(\boldsymbol{\rho})}}. \quad (14)$$

Applying this to the measured intensity pattern of Eq. (4), we obtain

$$I(\boldsymbol{\rho}; 0) \approx I_i(\boldsymbol{\rho}) + I_j(\boldsymbol{\rho}) + 2\sqrt{I_i(\boldsymbol{\rho})I_j(\boldsymbol{\rho})}|\bar{\mu}(\boldsymbol{\rho})|\cos[\Phi(\boldsymbol{\rho}, 0)]. \quad (15)$$

Therefore the overall spectral degree of coherence can be evaluated with only one temporal measurement point, which happens to be at zero time delay. Moreover, the approximation becomes better the more coherent the measured field is.

III. EXPERIMENTAL CONSIDERATIONS

In the following experiments, we employ a spectrally partially coherent source: a bulk-generated supercontinuum. We are interested in three operation regimes: at threshold, just above it, and strong pumping. To remove any coherence effects caused by the pump pulse, we generate supercontinuum pulses in two different sapphire plates, both of which are seeded with a copy of the same pump pulse. This is equivalent to generating a supercontinuum pulse train with a completely coherent pump pulse train, from which two different supercontinuum pulses are picked and interfered. Our approach is just far simpler to practically demonstrate, since the stability constraints on the pump pulse are lower, and there is no need for large delay lines to get subsequent pulses from the train. In the last set of our experiments, we also remove the pump wavelengths entirely, by employing a short-pass filter. This ensures that we are probing only the properties of the nonlinearly generated frequencies. Note that the pump power may be significantly higher than the supercontinuum power, since we are operating in the normal dispersion regime [24].

The experimental setup is illustrated in Fig. 1. We employ femtosecond pulses from a mode-locked Ti-sapphire laser (Continuum Integra C-5) as the pump. The laser has a center wavelength of 792 nm, approximately 8 nm spectral width, and 1 kHz repetition rate. The incident beam is passed through a spatial Gaussian apodizing filter (F) to generate a clean Gaussian beam of 5 mm width, and focused with a lens (L) of focal length of 300 mm. Using a 50:50 beam splitter (BS1; Thorlabs BS014), we divide the beam into two arms of a Mach-Zehnder-type interferometer, such that the split beams focus onto two 5-mm-thick sapphire plates (S1 and S2).

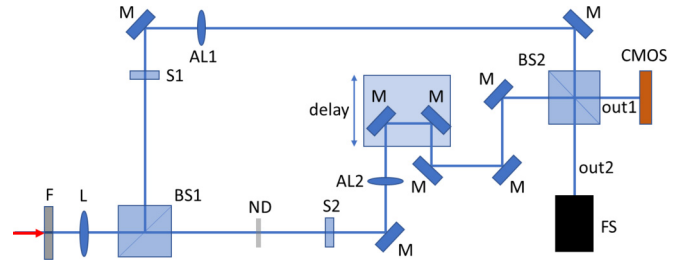


FIG. 1. Schematic diagram of the experimental setup. F, spatial Gaussian filter; L, focusing lens (300 mm); ND, neutral density filter with variable transmittance; S1 and S2, 5-mm-thick sapphire plates; AL1 and AL2, positive achromatic lenses of focal length 150 mm; M, mirror; BS1 and BS2, beam splitters; CMOS, camera; FS, fiber spectrometer; out1 and out2, outputs 1 and 2.

The overall power of the pump pulse is controlled before the input. To obtain identical pumping conditions at the two plates, we use the same lens to focus the beam in both arms (placed before BS1) and balance the intensities with a neutral density filter (ND) in one of the arms. After the plates, we use two achromatic lenses of focal length 150 mm (AL1 and AL2), to collimate the output supercontinuum beams. Delay is introduced to one of the arms with a piezoelectric translation stage (P-611.1S from PI Store), which has a step size of $\approx 10 \pm 2$ nm and a travel range of 100 μm .

The collimated beams are then superimposed on a camera [complementary metal-oxide semiconductor (CMOS); Thorlabs DCC1545M-GL] at output 1 of the second beam splitter (BS2; Thorlabs BSW26R). The alignment is done in such a way that the beam centers from both arms overlap with each other. Utilizing the last two mirrors of the second arm, we control the tilt angle of the beam, and hence the fringe width of the interference pattern on the camera without changing beam position. At output 2 we measure the power spectrum with a spectrometer (AvaSpec-2048).

Our setup can be used to measure the position-dependent cross-correlation function for various different pumping conditions. We adjust the power of the incident beam with a half-wave plate and a linear polarizer. Since the repetition rate of the femtosecond laser is 1 kHz, the pulse energies are particularly simple to find from the measured incident power. We measure the power after the first beam splitter (BS1 in Fig. 1) in both arms, which are listed in Table I.

TABLE I. Different pumping conditions. The pump pulse full width at half maximum (FWHM) is ≈ 200 fs, and the beam radius at the focal spot is ≈ 25 μm . The colors refer to the colors used in Fig. 3.

Power levels	Power (mW)	Energy (μJ)
Below threshold (red)	1.22	1.22
At threshold (green)	1.31	1.31
Above threshold (blue)	1.63	1.63
High pumping (black)	2.4	2.4

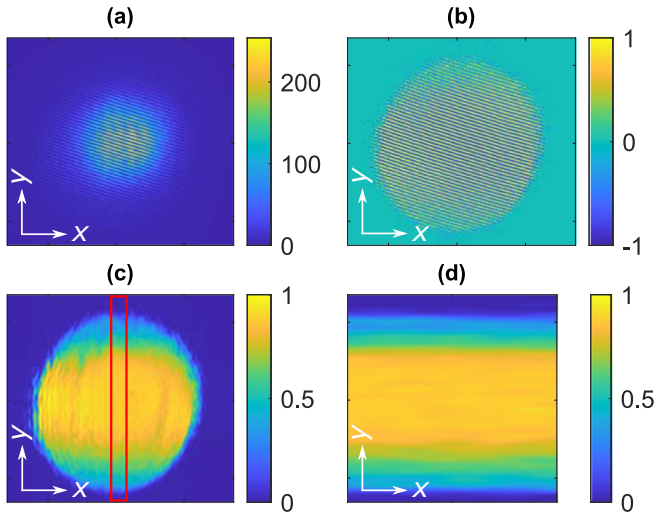


FIG. 2. Illustration of the measured interference fringes, at above-threshold pumping and zero delay at the center of the beam. (a) Observed interference $I(\rho)$, (b) normalized interference fringes $I_{\text{norm}}(\rho)$, (c) degree of coherence, and (d) cropped red marked part of (c) used further to calculate the intensity-normalized cross-correlation function.

IV. RESULTS

Allowing light only from the first arm measures $I_i(\rho)$, whereas $I_j(\rho)$ is found by blocking the other arm. Keeping both arms open produces the interference pattern $I(\rho; \Delta t)$, which we then normalize using the individual intensities

$$I_{\text{norm}}(\rho; \Delta t) = \frac{I(\rho; \Delta t) - I_i(\rho) - I_j(\rho)}{2\sqrt{I_i(\rho)I_j(\rho)}}. \quad (16)$$

We show a typical measured interference pattern at zero delay in Fig. 2(a) and the extraction of the degree of coherence in Figs. 2(b)–f(d). The fringes are removed with the use of standard Fourier signal processing techniques [25,26].

Once we get the normalized interference pattern, we pick a central location around $x = 0$, which is plotted in Fig. 2(d), and average a small segment along the x direction to get $|\bar{\mu}(0, y; \Delta t)|$. In our experiments, the fields were rotationally symmetric, and therefore measuring along the y axis yields the same information as $|\bar{\mu}(\rho; \Delta t)|$. The decrease in the overall degree of coherence along the y axis is due to crossed wave fronts, which causes position-dependent time delay. However, we can compensate for this by scanning the piezo stage, causing the maximum fringe visibility to move over the interference pattern. Note that there is no position-dependent time delay along the x axis in this particular setup, as can be seen from Fig. 2(c). Moreover, the position-dependent time delay could be entirely removed by setting the wave fronts parallel and scanning the delay instead to see the interference [27]. We repeat the measurement for the three different pumping conditions.

In Fig. 3(a), we demonstrate the measured normalized cross correlation as a function of delay at the beam center ($x = 0, y = 0$). Different colors in the figure correspond to different pumping levels. Looking at Fig. 3, one can immediately recognize that the overall degree of spectral coherence

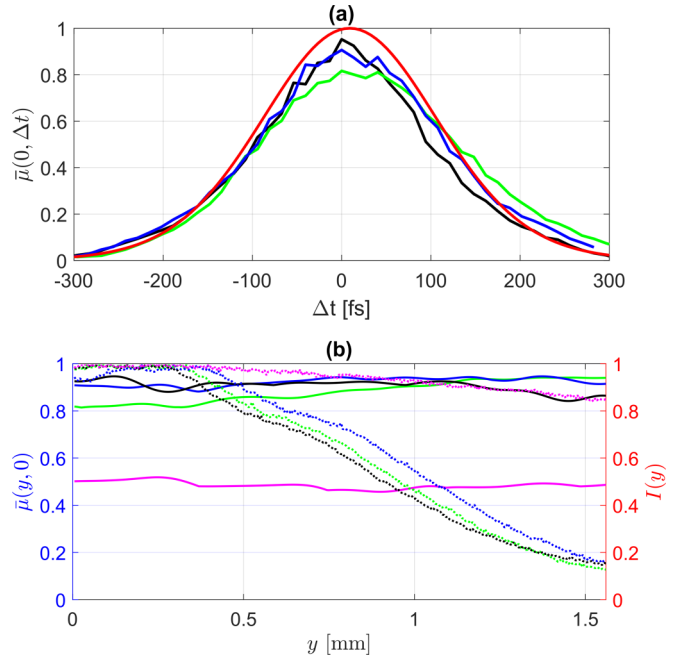


FIG. 3. (a) Measured intensity-normalized cross-correlation function at the beam center. Different colors represent different pumping conditions. Red, below threshold; green, at threshold; blue, above threshold; black, high pumping. (b) The overall degree of spectral coherence (solid lines) and intensity distribution (dotted lines) plotted against the left and right axes, respectively, as a function of position. The colors are otherwise the same as in (a), with one extra color for high pumping with a low-pass filter (magenta). The cross-correlation trace for the filtered high-pumping case is shown in Fig. 4, with substantially higher resolution.

($|\bar{\mu}(\rho, 0)|$) is close to unity for all considered pumping conditions. For the pump pulse only, the cross correlation reduces to the autocorrelation (red line) and the zero time delay corresponds to visibility near 1, as one would expect. However, we see a dip in the overall degree of coherence at threshold, and the coherence of the field increases as pumping is increased. This is in perfect agreement with Ref. [22].

Next, we introduce a short-pass filter at the output of the interferometer, with a cutoff wavelength of 750 nm (Thorlabs FESH0750) to remove the pump wavelengths in the high-pumping case. This dramatically changes the measured cross correlation, and the measured overall degree of spectral coherence goes down to $\bar{\mu} \approx 0.5$ [see Fig. 3(b)]. Unfortunately, our temporal delay axis does not contain enough data points for reliable direct retrieval of the quasicohherent part of the spectrum with Eq. (6). Therefore we investigate the spatial dependence of the supercontinuum to find out whether it is possible to extract more data by exploiting the time delay due to crossed wave fronts and return to the filtered case later.

In Fig. 3(b), we present the measured position-dependent overall degrees of spectral coherence for all considered pumping conditions. First, let us consider the unfiltered cases. Again, the overall trend in the measured degree of coherence is similar to what was found in Ref. [22]; the lowest coherence is found at the center of the beam when the pumping is at supercontinuum generation threshold. However, the drop

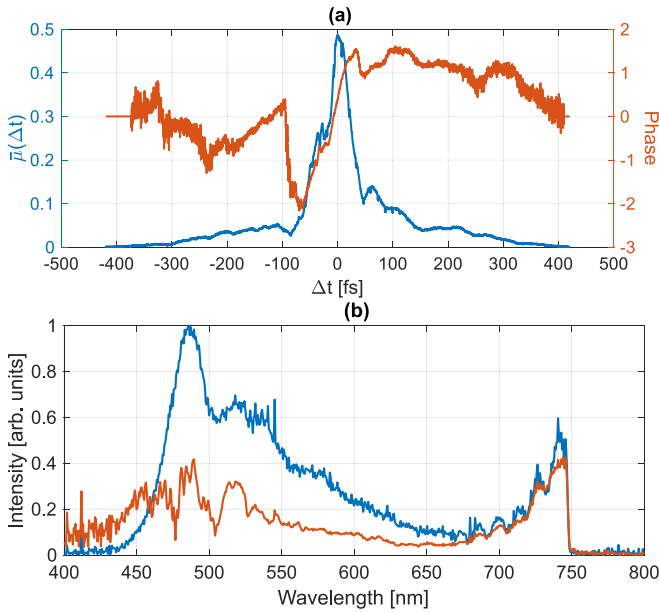


FIG. 4. (a) Measured cross-correlation trace for the high-pumping case after introducing a low-pass filter, where we have both the absolute value (blue), as well as the phase (red). (b) Measured power spectrum with low-pass filter (blue) and retrieved S_{qc} (red). The quasioherent contribution should never exceed the overall spectrum, and the short-wavelength end is dominated by noise.

in coherence is not as significant as what was predicted by numerical simulations. This is probably due to the slightly different pumping conditions compared with those in the numerical case, as we could not exactly duplicate them.

Moving on to the filtered case, we see that in this case the temporal properties are only weakly dependent on the spatial position (magenta line in Fig. 3), and therefore we can attain a very good approximation of the cross correlation by exploiting crossed wave fronts. Now, we handle the data slightly differently: We take the cross section along the y axis—which contains the temporal cross-correlation data due to the time delay along the y axis—for all piezo-stage-induced delays and extract the absolute value and phase with standard Fourier signal processing. We then take the data from each measurement and concatenate the extracted values. The absolute value was directly found with this method, whereas the (reduced) phase was found by removing a constant linear term. Only weak position dependence was found, and Fig. 4(a) depicts the retrieved values.

Next, we attempt to retrieve the quasioherent part of the spectrum with Eq. (6). In principle, the retrieval can be done with a simple fast Fourier transform. However, since our bandwidth is quite large (~ 300 nm), the cross-correlation trace has to be measured with very good resolution. The employed piezo stage can reach such resolution, but the rest of the setup is susceptible to vibration. Therefore the time domain signal forms a convolution between vibration noise and the quasioherent part of the spectrum, and a lot of the temporal resolution is lost. Doing a direct fast Fourier transform on the data presented in Fig. 4(a) results in a quasioherent spectrum which shows only the filter edge. This is because the longer

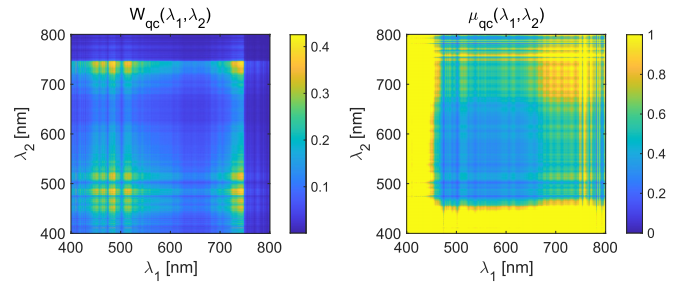


FIG. 5. Constructed W_{qc} and μ_{qc} . The degree of coherence attains values higher than unity below ~ 475 nm, but as this is not physically possible, any values above 1 are cut off.

wavelengths do not require as good resolution as the shorter ones.

Thankfully, we have two additional data constraints that can be used to deconvolve the quasioherent part of the spectrum from the vibration noise. First, we know that the overall degree of coherence has to be on the order of $\bar{\mu} \approx 0.5$, and according to Eq. (11), this means that the quasioherent part of the field has about half of the energy of the total field. Second, we observed that the fringe spacing changed when the filter was introduced. The spacing is determined by the central frequency of the field, which was found to be about 635 nm in the filtered case. Since time domain convolution is equal to frequency domain multiplication, we can deconvolve the data by dividing the retrieved S_{qc} with a Gaussian noise spectrum, such that the position and width are fixed by the two additional constraints.

The retrieved quasioherent part of the spectrum is found in Fig. 4(b), together with the overall spectrum measured with a spectrometer. As can be seen from the figure, the spectral coherence is greatest near the pump, and it decreases toward shorter wavelengths. The signal-to-noise ratio of the retrieved S_{qc} also decreases when moving towards shorter wavelengths, and from ~ 475 nm onward, noise becomes dominant. There is no method to remove this noise, since the deconvolution increases the noise floor as well. Therefore the blue end of the quasioherent spectrum does not reliably reproduce the coherence properties of the field.

Finally, we employ the retrieved S_{qc} to form the quasioherent part of the CSD as well as the quasioherent part of the spectral degree of coherence, as outlined in Eqs. (8) and (9) (Fig. 5). Due to increasing noise power toward shorter wavelengths, the results are reliable only up to ~ 475 nm, after which the field gains impossibly high coherence ($\mu_{qc} > 1$).

V. DISCUSSION AND CONCLUSIONS

In this paper, we have first theoretically established that the cross-correlation technique introduced in Ref. [21] can be used to find the overall degree of spectral coherence in a single measurement. Furthermore, we have experimentally demonstrated the cross correlation by measuring the bulk-generated supercontinuum and consequently confirmed the theoretical predictions made in Refs. [21,22]. The qualitative agreement between the earlier numerical results and the experimental results presented here is very good, with both

showing similar features. For example, there is a dip in the overall degree of coherence at the supercontinuum generation threshold in the center of the beam, and the overall degree of coherence increases with increasing pump power. These features are exactly the same as what was found in numerical simulations, although the dip in overall degree of coherence is not as large. This can be attributed to the differences between the experiment and simulation pumping conditions, since we could not exactly replicate the numerical parameters.

After confirming the results from our earlier studies, we went on to characterize the properties of the bulk-generated supercontinuum in more detail. This was accomplished by placing a short-pass filter at the output of the interferometer, which removed all of the pump power, and therefore we could measure frequencies that were nonlinearly generated. This caused the measured overall degree of coherence to plummet from near unity to about $\bar{\mu} \approx 0.5$. The sharp decrease in the spectral coherence shows that the majority of the correlations in the field were due to the pump pulse. This would suggest that the increase in coherence as pumping is increased is mainly due to a saturation of the supercontinuum generation, and the nonlinear efficiency decreases with increasing power density.

The data attained from the cross-correlation measurements were then used to retrieve S_{qc} and later employed to form W_{qc} , as well as μ_{qc} . By examining the correlation functions and the spectra, it is evident that the majority of the coherent contribution is near the pump, which is produced by anti-Stokes shift. On the other hand, the higher frequencies generated by self-phase modulation [23] feature a degree of

coherence below 0.5 for all wavelength pairs, and the highest power peak located at ~ 490 nm features a degree of coherence on the order of ~ 0.3 . Hence our results suggest that in the case of bulk-generated supercontinuum, stimulated Raman scattering is a coherent process, whereas self-phase modulation driven broadening causes incoherence. This is rather surprising, since the roles of these two nonlinear effects are reversed when comparing with the supercontinuum generated in a normal dispersion fiber [24]. Our results apply to a pump pulse of about 200 fs length, and a more detailed study of the effect of pump pulse duration may give further insight into these properties.

In conclusion, we have experimentally established a method for relatively simple retrieval of spectral coherence properties, from measured time domain data. The quasicohherent part of the correlation function can be retrieved even for a supercontinuum source, although it requires deconvolution steps if the setup is not ultrastable. More importantly, it is possible to find the overall degree of spectral coherence of the field with a single simple measurement. This allows for extremely fast evaluation of the stability of the field, which is crucial for generating short pulses and stable frequency combs.

ACKNOWLEDGMENTS

The authors acknowledge the financial support of the Academy of Finland Flagship Programme (PREIN-Decisions No. 320165 and No. 320166) and Academy of Finland Projects No. 322002 and No. 333938.

-
- [1] A. Forbes, *Laser Beam Propagation: Generation and Propagation of Customized Light* (CRC Press, Boca Raton, FL, 2014).
 - [2] G. Genty, M. Surakka, J. Turunen, and A. T. Friberg, Second-order coherence of supercontinuum light, *Opt. Lett.* **35**, 3057 (2010).
 - [3] G. Genty, M. Surakka, J. Turunen, and A. T. Friberg, Complete characterization of supercontinuum coherence, *J. Opt. Soc. Am. B* **28**, 2301 (2011).
 - [4] R. Dutta, A. T. Friberg, G. Genty, and J. Turunen, Two-time coherence of pulse trains and the integrated degree of temporal coherence, *J. Opt. Soc. Am. A* **32**, 1631 (2015).
 - [5] R. Dutta, J. Turunen, G. Genty, and A. T. Friberg, Temporal coherence characterization of supercontinuum pulse trains using Michelson's interferometer, *Appl. Opt.* **55**, B72 (2016).
 - [6] H. Lajunen, J. Tervo, J. Turunen, P. Vahimaa, and F. Wyrowski, Spectral coherence properties of temporally modulated stationary light sources, *Opt. Express* **11**, 1894 (2003).
 - [7] H. Lajunen, J. Tervo, and P. Vahimaa, Overall coherence and coherent-mode expansion of spectrally partially coherent plane-wave pulses, *J. Opt. Soc. Am. A* **21**, 2117 (2004).
 - [8] H. Lajunen, P. Vahimaa, and J. Tervo, Theory of spatially and spectrally partially coherent pulses, *J. Opt. Soc. Am. A* **22**, 1536 (2005).
 - [9] R. Trebino, *Frequency-Resolved Optical Gating: The Measurement of Ultrashort Laser Pulses* (Kluwer, Boston, 2000).
 - [10] C. Iaconis and I. A. Walmsley, Spectral phase interferometry for direct electric-field reconstruction of ultrashort optical pulses, *Opt. Lett.* **23**, 792 (1998).
 - [11] I. A. Walmsley and C. Dorrer, Characterization of ultrashort electromagnetic pulses, *Adv. Opt. Photon.* **1**, 308 (2009).
 - [12] M. Närhi, J. Turunen, A. T. Friberg, and G. Genty, Experimental Measurement of the Second-Order Coherence of Supercontinuum, *Phys. Rev. Lett.* **116**, 243901 (2016).
 - [13] P. Pääkkönen, J. Turunen, P. Vahimaa, A. T. Friberg, and F. Wyrowski, Partially coherent Gaussian pulses, *Opt. Commun.* **204**, 53 (2002).
 - [14] V. V. Kozlov, N. N. Rosanov, and S. Wabnitz, Obtaining single-cycle pulses from a mode-locked laser, *Phys. Rev. A* **84**, 053810 (2011).
 - [15] V. V. Kozlov and N. N. Rosanov, Single-cycle-pulse passively-mode-locked laser with inhomogeneously broadened active medium, *Phys. Rev. A* **87**, 043836 (2013).
 - [16] T. Udem, J. Reichert, R. Holzwarth, and T. W. Hänsch, Accurate measurement of large optical frequency differences with a mode-locked laser, *Opt. Lett.* **24**, 881 (1999).
 - [17] T. Udem, R. Holzwarth, and T. W. Hänsch, Optical frequency metrology, *Nature (London)* **416**, 233 (2002).
 - [18] V. Torres-Company, H. Lajunen, and A. T. Friberg, Effects of partial coherence on frequency combs, *J. Eur. Opt. Soc. Rapid Publ.* **2**, 070071-4 (2007).

- [19] N. R. Newbury and W. C. Swann, Low-noise fiber-laser frequency combs, *J. Opt. Soc. Am. B* **24**, 1756 (2007).
- [20] S. Koke, C. Grebing, H. Frei, A. Anderson, A. Assion, and G. Steinmeyer, Direct frequency comb synthesis with arbitrary offset and shot-noise-limited phase noise, *Nat. Photon.* **4**, 462 (2010).
- [21] M. Koivurova, L. Ahad, G. Geloni, T. Setälä, J. Turunen, and A. T. Friberg, Interferometry and coherence of nonstationary light, *Opt. Lett.* **44**, 522 (2019).
- [22] A. Halder, V. Jukna, M. Koivurova, A. Dubietis, and J. Turunen, Coherence of bulk-generated supercontinuum, *Photon. Res.* **7**, 1345 (2019).
- [23] J. M. Dudley, G. Genty, and S. Coen, Supercontinuum generation in photonic crystal fiber, *Rev. Mod. Phys.* **78**, 1135 (2006).
- [24] A. M. Heidt, J. S. Feehan, J. H. V. Price, and T. Feurer, Limits of coherent supercontinuum generation in normal dispersion fibers, *J. Opt. Soc. Am. B* **34**, 764 (2017).
- [25] M. Koivurova, H. Partanen, J. Lahyani, N. Cariou, and J. Turunen, Scanning wavefront folding interferometers, *Opt. Express* **27**, 7738 (2019).
- [26] A. Halder, H. Partanen, A. Leinonen, M. Koivurova, T. K. Hakala, T. Setälä, J. Turunen, and A. T. Friberg, Mirror-based scanning wavefront-folding interferometer for coherence measurements, *Opt. Lett.* **45**, 4260 (2020).
- [27] A. Efimov, Lateral-shearing, delay-dithering Mach–Zehnder interferometer for spatial coherence measurement, *Opt. Lett.* **38**, 4522 (2013).